

Four-loop two-mass tadpoles and the ρ parameter

Samuel Abreu,^{a,b} Arnd Behring,^{a,*} Andrew McLeod^{a,b} and Ben Page^{a,c}

^a*Theoretical Physics Department, CERN,
1211 Geneva 23, Switzerland*

^b*Higgs Centre for Theoretical Physics, School of Physics and Astronomy,
The University of Edinburgh, Edinburgh EH9 3FD, Scotland, UK*

^c*Department of Physics and Astronomy, Ghent University,
9000 Ghent, Belgium*

E-mail: arnd.behring@cern.ch

We calculate four-loop QCD corrections to the electroweak ρ parameter with a non-vanishing b quark mass. At three loops, it was observed that elliptic integrals contribute to this observable. This prompts the question of which classes of functions appear at the next order. We report on the status of our calculation with a focus on the mathematical structures that emerge at four loops.

*Loops and Legs in Quantum Field Theory (LL2024)
14–19 April 2024
Wittenberg, Germany*

*Speaker

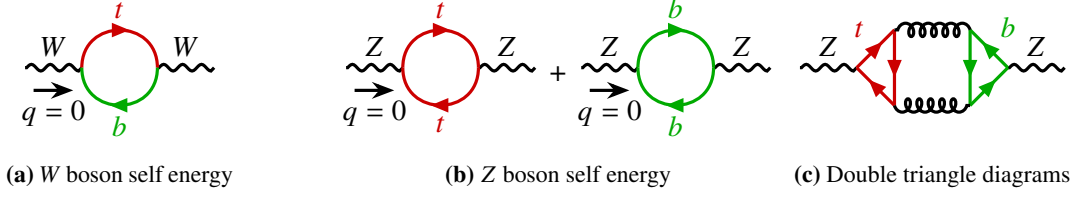


Figure 1: Fermionic diagrams that contribute to the W and Z boson self energies.

1. Introduction

The ρ parameter is an important electroweak precision observable. It was introduced by Ross and Veltman in 1975 [1] to distinguish the Weinberg model, i.e., what turned into the modern Standard Model, from alternative scenarios with extended Higgs sectors. Over the years, the ρ parameter has proven to be a valuable tool for precision tests of the electroweak gauge sector of the Standard Model. The ρ parameter is defined as

$$\rho = \frac{m_W^2}{m_Z^2 \cos^2 \theta_W}, \quad (1)$$

where m_W and m_Z are the masses of the W and Z boson, respectively, and θ_W is the weak mixing angle. At tree level in the Standard Model we have $\rho = 1$, but in New Physics scenarios ρ can differ from 1 substantially. Also within the Standard Model, higher-order contributions cause the ρ parameter to deviate slightly from its tree-level value. There exists a long history of calculations that address these higher-order corrections in the Standard Model, starting with the calculation of one-loop corrections by Veltman [2]. From there, one can compute corrections at higher orders in the strong coupling α_s [3–15] or the electroweak coupling α [16–20], or both [20].

While calculating the three-loop QCD corrections with two non-vanishing quark masses, it was observed that elliptic integrals appear [10–12]. As also integrals over more complicated geometries such as hyperelliptic curves and Calabi-Yau manifolds are known to appear in perturbative quantum field theory [21], it thus becomes natural to ask: what types of integrals appear at four loops?

Corrections to the ρ parameter can be expressed as the difference between the Z and W boson self energies,

$$\rho = 1 + \Delta\rho, \quad \Delta\rho = \frac{\Sigma_Z(q^2 = 0)}{m_Z^2} - \frac{\Sigma_W(q^2 = 0)}{m_W^2}. \quad (2)$$

In the Standard Model, the fermionic one-loop correction to the W boson self energy just consists of one Feynman diagram: a one-loop fermionic bubble with up- and down-type quarks connecting the W boson vertices. The Z boson self energy receives contributions from two diagrams, in which only one flavour appears in the fermion loop. These diagrams are shown in Figs. 1a and 1b. Due to the $SU(2)_L$ structure of the W boson coupling to fermions, QCD corrections to the W boson self energy just add quark loops and gluons to the one-loop diagram. Similarly, the majority of QCD corrections to Z boson self energy are found by dressing the one-loop diagrams with quark loops and gluons, except that, starting from three-loop order, also double triangle diagrams appear (see Fig. 1c).

The self energies in $\Delta\rho$ are evaluated for vanishing external momentum, $q = 0$, which means that the Feynman integrals are tadpole integrals. They can be mapped to a small number of topologies (one topology each at one-, two- and three-loop order, and two topologies at four-loop order). However, this requires us to distinguish different mass labellings of each topology. After generating the diagrams using QGRAF [22], we use FORM [23] to insert Feynman rules, apply projectors to extract the transversal part of the self energies and to simplify the colour and Dirac algebra. We use integration-by-parts (IBP) relations [24–26] via REDUZE2 [27] to reduce the integrals to a smaller set of master integrals. The master integrals can be calculated using the method of differential equations in the mass ratio $x = \frac{m_b}{m_t}$. In order to obtain numerical values for the master integrals, we also use AMFLOW [28–31].

The numerical impact of the four-loop two-mass QCD corrections is expected to be very small. Indeed, our main motivation for performing this calculation is the question of which classes of functions are necessary to express the solutions. Up to two-loop order, only harmonic polylogarithms are necessary to express the two-mass corrections. At three-loop order, it was observed in Ref. [10] that elliptic integrals appear. The explicit analytic result in terms of iterated integrals was later obtained in Refs. [11, 12]. It is thus natural to ask what happens at four-loop order: will new classes of functions appear? Do we, for example, encounter multiple elliptic curves, higher-genus curves, or higher-dimensional geometries? We will address these questions in these proceedings.

2. Analysis

After IBP reduction, we end up with 283 master integrals that can be organised into 197 sectors. Many of these integrals are polylogarithmic, or can be expressed in terms of polylogarithmic functions after rationalising a square root. In order to identify which functions appear beyond multiple polylogarithms, we need a criterion to narrow down the number of sectors that we have to analyse in more detail. To this end, we analyse the differential equations. In particular, we use the fact that new structures arise from the homogeneous part of the differential equation.¹ That means that it is sufficient to consider the differential equations in the limit $\epsilon \rightarrow 0$ and at the level of maximal cuts. We derive the Picard-Fuchs operator by uncoupling the first-order differential equation systems into a single higher-order differential equation for one of the integrals of the sector. There are algorithms and packages that automate this step [32–34]. We then try to find a factorisation of the differential operator, for example using MAPLE’s DFactor command [35]. If it is possible to find a factorisation into first-order factors, we can exclude that new structures arise from this sector. However, if factors of order two or higher appear, we take this as an indication that non-polylogarithmic structures can emerge and that we need to analyse this sector in more detail. We note that finding higher-order factors is not a sufficient criterion for the appearance of elliptic integrals or generalisations thereof, as we will see below.

Analysing the 197 sectors in this way lets us identify 15 sectors at four loops that we have to analyse in more detail. Only eight of these sectors are independent after taking into account permutations of m_b and m_t , which do not change the class of functions. This leaves us with eight

¹Integrals can depend on elliptic curves and more general geometries also through subtopologies. Since we consider all sectors of master integrals that appear in the calculation and since at this point we are only interested in surveying the new mathematical structures that appear, we can restrict ourselves to investigating only the maximal cuts.

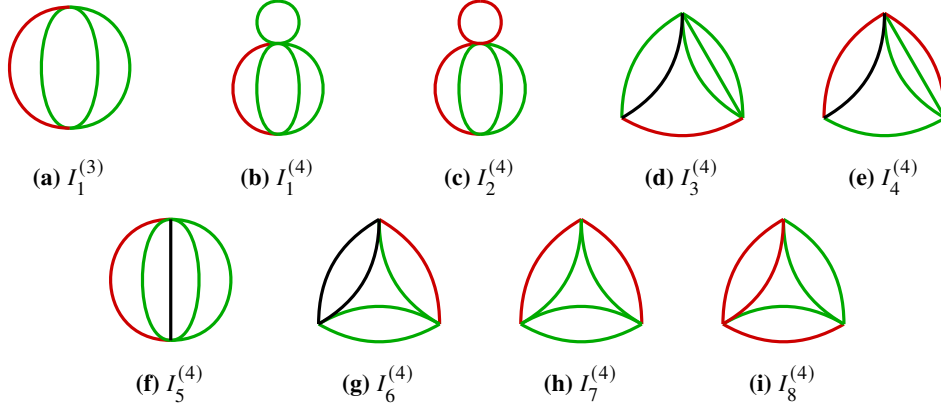


Figure 2: Representative diagrams for integrals from sectors that we identified as potentially elliptic. Black solid lines represent massless propagators, green and red lines represent massive propagators with mass m_b and m_t , respectively. For integrals $I_1^{(3)}$ and $I_{1,\dots,7}^{(4)}$ there exist corresponding integrals $\tilde{I}_1^{(3)}$ and $\tilde{I}_{1,\dots,7}^{(4)}$ that are related by swapping $m_b \leftrightarrow m_t$. Integral $I_8^{(4)}$ is symmetric under this transformation.

sectors to analyse in detail. Representative diagrams for each sector are shown in Fig. 2. All of these sectors have Picard-Fuchs operators of order two, three or four. In each case we find at most second-order factors when trying to factorise the differential operators using DFactor.

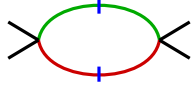
We further analyse the sectors by considering the maximal cut of their integrals in $d = 2$ dimensions since they fulfil homogeneous differential equations [36, 37]. We work in loop-by-loop Baikov representation [38, 39] as this allows us to reuse building blocks from lower orders to construct the maximal cuts. In order to identify non-polylogarithmic integrals, we investigate the geometric structure of the maximal cuts. For example, integrals that depend on elliptic curves show up as $\int \frac{dz}{y}$ with $y^2 = P(z)$, where $P(z)$ is a polynomial of degree 3 or 4. If $P(z)$ is a degree- n polynomial, this would correspond to a genus- $\lfloor \frac{n-1}{2} \rfloor$ curve. Higher-dimensional structures, such as Calabi-Yau manifolds, would show up as multivariate integrals over algebraic functions.

Before analysing these four-loop topologies, we collect some results about maximal cuts of one- and two-loop integrals. We will use these results as building blocks later in the analysis, and to help us interpret our findings. At one loop, we are interested in bubble integrals, which we will denote by $B_{ij}(q^2)$, where $i, j \in \{0, b, t\}$ denote the masses of the two internal propagators and q is the external momentum flowing through the two-point integral. Up to irrelevant numerical prefactors, the maximal cut of the one-loop bubble integrals are given by

$$\text{MaxCut } B_{00}(q^2) = \text{diagram} \sim \frac{1}{q^2}, \quad (3)$$

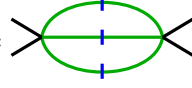
$$\text{MaxCut } B_{b0}(q^2) = \text{diagram} \sim \frac{1}{q^2 - m_b^2}, \quad (4)$$

$$\text{MaxCut } B_{bb}(q^2) = \text{diagram} \sim \frac{1}{\sqrt{q^2[q^2 - 4m_b^2]}}, \quad (5)$$



$$\text{MaxCut } B_{bt}(q^2) = \text{Diagram} \sim \frac{1}{\sqrt{[q^2 - (m_b - m_t)^2][q^2 - (m_b + m_t)^2]}}. \quad (6)$$

We see that the maximal cut of the massless bubble $B_{00}(q^2)$ takes the form of a massless propagator and that of the single-mass bubble $B_{b0}(q^2)$ looks like a massive propagator. The maximal cuts of the equal-mass and unequal-mass bubbles, $B_{bb}(q^2)$ and $B_{bt}(q^2)$, already contain square roots. Considering the maximal cut of the equal-mass sunrise $S_{bbb}(q^2)$, we find [40]²



$$\text{MaxCut } S_{bbb}(q^2) = \text{Diagram} \sim \int \frac{dz}{\sqrt{\left[z - (\sqrt{q^2} - m_b)^2\right] \left[z - (\sqrt{q^2} + m_b)^2\right]} \sqrt{z[z - 4m_b^2]}}. \quad (7)$$

In contrast to the previous examples, the maximal cut of the sunrise integral is not just rational or algebraic functions but actually an elliptic integral.

Let us now consider $I_1^{(3)}$ (see Fig. 2a), an integral which contributes to the three-loop two-mass corrections to the ρ parameter, which was called $J_{8b}^{(3)}$ in Ref. [10]. We can think of this integral as two one-loop bubble integrals that are inserted onto a one-loop tadpole. This leads to the representation

$$I_1^{(3)} \sim \int d^d k B_{bt}(k^2) B_{bb}(k^2). \quad (8)$$

The integration over k corresponds to the integration over the loop momentum of the one-loop tadpole. Inserting the building blocks for the maximal cuts of the one-loop bubbles we discussed before and using the fact that the integrand only depends on k^2 to perform the spherical part of the loop integration, we find

$$\text{MaxCut } I_1^{(3)} \sim \int \frac{dk^2}{\sqrt{[k^2 - (m_t - m_b)^2] [k^2 - (m_t + m_b)^2]} \sqrt{k^2[k^2 - 4m_b^2]}}. \quad (9)$$

Comparing this expression to Eq. (7), we see that this is exactly the maximal cut of the on-shell ($q^2 = m_t^2$) two-loop sunrise integral. We will call the elliptic curve that appears here the *sunrise curve* due to this connection. Obviously, there exists a related integral $\tilde{I}_1^{(3)}$ that emerges upon swapping m_b and m_t . The elliptic curve that shows up in that integral will be called the *sunrise twin curve*.

We are now ready to discuss a few examples at four-loop order. The first integral, $I_3^{(4)}$ (see Fig. 2d), can be read as a propagator, a single-mass bubble and an equal-mass sunrise integral inserted on a one-loop tadpole,

$$I_3^{(4)} \sim \int d^d k B_{b0}(k^2) \frac{1}{k^2 - m_t^2} S_{bbb}(k^2). \quad (10)$$

²Here and in the following, we do not explicitly specify the integration contour. Each independent contour yields a linearly independent solution to the homogeneous differential equation. However, the specific contour is not relevant to our discussion.

Taking the maximal cut of this integral leads to

$$\text{MaxCut } I_3^{(4)} \sim \int dk^2 \frac{\delta(k^2 - m_t^2)}{k^2 - m_b^2} \int \frac{dz}{\sqrt{[z - (\sqrt{k^2} - m_b)^2] [z - (\sqrt{k^2} + m_b)^2] \sqrt{z [z - 4m_b^2]}}}. \quad (11)$$

The δ distribution corresponds to the maximal cut of the single propagator, the propagator-like factor $(k^2 - m_b^2)^{-1}$ is the maximal cut of the single-mass bubble and the remaining integral over z comes from the maximal cut of the sunrise integral. The integral over the tadpole loop momentum k can be performed with the help of the δ distribution and we arrive at

$$\text{MaxCut } I_3^{(3)} \sim \frac{1}{m_t^2 - m_b^2} \int \frac{dz}{\sqrt{[z - (m_t - m_b)^2] [z - (m_t + m_b)^2] \sqrt{z [z - 4m_b^2]}}}. \quad (12)$$

Inspecting the result reveals that this integral also depends on the sunrise elliptic curve.

As a second example, we consider $I_6^{(4)}$ (see Fig. 2g), an integral that consists of three bubble integrals chained together in a loop. We call integrals with this kind of topology *necklace integrals* and we will return to them below. The three bubbles are a massless bubble, an equal-mass bubble and an unequal-mass bubble,

$$I_6^{(4)} \sim \int d^d k B_{00}(k^2) B_{bb}(k^2) B_{bt}(k^2). \quad (13)$$

The maximal cut of this integral reads

$$\text{MaxCut } I_6^{(4)} \sim \int \frac{dz}{z \sqrt{[z - (m_t - m_b)^2] [z - (m_t + m_b)^2] \sqrt{z [z - 4m_b^2]}}}, \quad (14)$$

which, upon comparison with Eq. (7), again turns out to be related to the sunrise curve.

Our next example looks very similar superficially, but turns out to exhibit different behaviour. The integral $I_7^{(4)}$ (see Fig. 2h) contains two unequal-mass bubbles and one equal-mass bubble chained into a loop,

$$I_7^{(4)} \sim \int d^d k B_{bt}^2(k^2) B_{bb}(k^2), \quad (15)$$

and its maximal cut takes the form

$$\text{MaxCut } I_7^{(4)} \sim \int \frac{dz}{[z - (m_t - m_b)^2] [z - (m_t + m_b)^2] \sqrt{z [z - 4m_b^2]}}. \quad (16)$$

Since the unequal-mass bubble appears twice, its contribution to the maximal cut becomes squared, which turns the two branch points of the square root appearing in the maximal cut of the bubble into simple poles of the full integral. This reduces the degree of the polynomial under the square root from four to two, which means that the maximal cut of this integral is not an elliptic integral,

but just an algebraic function. Thus, integral $I_7^{(4)}$ serves as an example where the appearance of a second-order factor in the Picard-Fuchs operator does not automatically imply an elliptic solution.³

The final example we want to discuss here is $I_8^{(4)}$ (see Fig. 2i), an integral that consists of three bubbles, two equal-mass bubbles that however each depend on different masses, and one unequal-mass bubble,

$$I_8^{(4)} \sim \int d^d k B_{tt}(k^2) B_{bb}(k^2) B_{bt}(k^2), \quad (17)$$

whose maximal cut is

$$\text{MaxCut } I_8^{(4)} \sim \int \frac{dz}{z \sqrt{[z - 4m_t^2]} \sqrt{[z - 4m_b^2]} \sqrt{[z - (m_t - m_b)^2]} \sqrt{[z - (m_t + m_b)^2]}}. \quad (18)$$

While this integral also features a degree-4 polynomial under the square root and yields an elliptic integral, the elliptic curve that appears is related neither to the sunrise curve nor to the sunrise twin curve.

Overall we find from our analysis that three different elliptic curves appear in the integrals: the sunrise curve, the sunrise twin curve, and the new curve that shows up in integral $I_8^{(4)}$. The curves are defined by $y^2 = P_i(z)$ with

$$P_1(z) = z [z - 4m_b^2] [z - (m_t - m_b)^2] [z - (m_t + m_b)^2], \quad (\text{sunrise curve}) \quad (19)$$

$$P_2(z) = z [z - (m_t - m_b)^2] [z - (m_t + m_b)^2] [z - 4m_t^2], \quad (\text{sunrise twin curve}) \quad (20)$$

$$P_3(z) = [z - 4m_b^2] [z - (m_t - m_b)^2] [z - (m_t + m_b)^2] [z - 4m_t^2]. \quad (\text{new curve}) \quad (21)$$

We find the following classification

$$\begin{aligned} I_1^{(3)}, I_{1,\dots,6}^{(4)} &\rightsquigarrow P_1(z), & \tilde{I}_1^{(3)}, \tilde{I}_{1,\dots,6}^{(4)} &\rightsquigarrow P_2(z), \\ I_7^{(4)}, \tilde{I}_7^{(4)} &\rightsquigarrow \text{non-elliptic}, & I_8^{(4)} &\rightsquigarrow P_3(z). \end{aligned}$$

We have checked by computing the j invariant of the curves that they are not isomorphic to each other, see, e.g., Ref. [41] for details. Moreover, we verified that the curves are not isogenic by computing the periods numerically for randomly chosen values of the masses.

The maximal cut analysis in loop-by-loop Baikov representation has the additional advantage that it reveals an intuitive physical interpretation of the branch points of the elliptic curves. The branch points of the square roots in the maximal cuts of the one-loop bubbles correspond to the thresholds and pseudothresholds of these integrals. Since the final integration of the four-loop integrals corresponds to the square of the loop momentum k that flows through the bubble integrals, we can interpret the branch points of the elliptic curves also as thresholds or pseudothresholds in the internal loop momentum space. Given two different masses, there are in total five different

³We remark that the differential variable influences whether we find an irreducible second-order factor the Picard-Fuchs operator: trying to factorize the differential operator for integral $I_7^{(4)}$ in $x^2 = m_b^2/m_t^2$, as we first did, yields a second-order factor, while the operator in x actually fully factorises into first-order factors. This is due to the restriction that the algorithm behind the DFactor command works over the field of rational functions in the differential variable. We chose to keep this example to point out this important caveat.

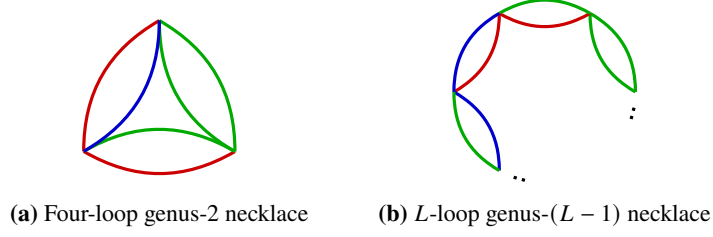


Figure 3: Example diagrams that give rise to Feynman integrals that depend on higher-genus curves.

(pseudo)thresholds and, indeed, each of the three curves uses four of those five thresholds as its branch points.

Thus far, we have only analysed the maximal cuts of the integrals that contribute to the four-loop ρ parameter. In order to gain a fuller picture of the class of functions that are necessary to express the result, we also have to take into account how the inhomogeneous parts of the differential equations couple different integrals to each other. In the three-loop calculation, two elliptic curves appeared, but sectors featuring different curves were never coupled to each other and individual integrals always only depended on a single elliptic curve. Therefore, it is possible to express the result in terms of elliptic multiple polylogarithms [12].⁴ However, in the calculation at hand, we find that integrals which depend on the three different elliptic curves we identified are coupled to each other by the differential equations. This implies that elliptic multiple polylogarithms may not be not sufficient to express the results.

Finally, let us comment on how generalized versions of some of the diagrams that contribute to the ρ parameter give rise to integrals over *hyperelliptic* curves. In particular, the diagrams in Figs. 2g to 2i can be thought of as degenerations of the four-loop necklace diagram shown in Fig. 3a. When we have particles with only two different masses appearing in this integral, the number of branch points is constrained by combinatorics. That is, the pseudothresholds of equal-mass bubbles necessarily agree ($m_b - m_b = m_t - m_t = 0$). Therefore, we can only construct curves with at most four non-repeated roots. However, if we allow for three different masses, we could combine two different unequal-mass bubbles and an equal-mass bubble, see Fig. 3a, to generate a degree-6 polynomial,

$$y^2 = z [z - 4m_b^2] [z - (m_t - m_b)^2] [z - (m_t + m_b)^2] [z - (m_t - m_3)^2] [z - (m_t + m_3)^2], \quad (22)$$

and thus a genus-2 curve.

Going beyond four-loop order, we can even construct L -loop integrals that give rise to integrals over a genus- $(L - 1)$ curve as their maximal cuts. Similar to the construction above, we chain $(L - 1)$ one-loop bubbles into a loop, while ensuring that the mass assignment is such that none of the thresholds or pseudothresholds coincide, see Fig. 3b. The maximal cut of an integral constructed in this way will depend on a genus- $(L - 1)$ curve. We note that the minimal number of masses that are necessary to ensure distinct branch points grows rather slowly. These integrals represent an interesting class of examples and can serve as toy models for studying integrals that depend on higher-genus curves and show up as soft limits of integrals that contribute to the Standard Model.

⁴Alternatively, it is possible to express the result in terms of iterated integrals over kernels involving hypergeometric ${}_2F_1$ functions [11, 42].

3. Conclusions and outlook

We have reported on our ongoing calculation of the two-mass QCD contributions to the four-loop ρ parameter. This is an interesting testing ground for which special functions appear in Standard Model observables. We find three distinct elliptic curves that contribute to the integrals and observe that the differential equations couple integrals that depend on different elliptic curves. This poses challenges for finding analytic closed form solutions to these Feynman integrals.

Starting from the expressions for the weak boson self energies in terms of master integrals, it is straightforward to calculate a numerical value for these four-loop corrections. However, since the tadpole integrals are universal building blocks that can be useful also for other calculations, we will calculate series representations that yield results for arbitrary values of the masses. In the long term, it would be interesting to investigate how to effectively and efficiently express the tadpole integrals in terms of special functions with known properties. Finally, we also plan to study necklace integrals with more than two masses as examples for Feynman integrals that depend on higher-genus curves.

Acknowledgements

The work of AM has been supported by the Royal Society grant URF\R1\221233. The work of BP has received funding from the European's Union Horizon 2020 research and innovation programme LoopAnsatz (grant agreement number 896690).

References

- [1] D. A. Ross and M. J. G. Veltman, *Neutral Currents in Neutrino Experiments*, *Nucl. Phys. B* **95** (1975) 135–147.
- [2] M. J. G. Veltman, *Limit on Mass Differences in the Weinberg Model*, *Nucl. Phys. B* **123** (1977) 89–99.
- [3] A. Djouadi and C. Verzegnassi, *Virtual Very Heavy Top Effects in LEP / SLC Precision Measurements*, *Phys. Lett. B* **195** (1987) 265–271.
- [4] A. Djouadi, *$O(\alpha_s)$ Vacuum Polarization Functions of the Standard Model Gauge Bosons*, *Nuovo Cim. A* **100** (1988) 357.
- [5] B. A. Kniehl, J. H. Kühn and R. G. Stuart, *QCD Corrections, Virtual Heavy Quark Effects and Electroweak Precision Measurements*, *Phys. Lett. B* **214** (1988) 621–629.
- [6] B. A. Kniehl, *Two Loop Corrections to the Vacuum Polarizations in Perturbative QCD*, *Nucl. Phys. B* **347** (1990) 86–104.
- [7] A. Anselm, N. Dombey and E. Leader, *Role of the axial anomaly in the Z_0 mass*, *Phys. Lett. B* **312** (1993) 232–234.
- [8] L. Avdeev, J. Fleischer, S. Mikhailov and O. Tarasov, *$O(\alpha_s^2)$ correction to the electroweak ρ parameter*, *Phys. Lett. B* **336** (1994) 560–566, [hep-ph/9406363], [Erratum: *Phys. Lett. B* **349** (1995) 597–598].

- [9] K. G. Chetyrkin, J. H. Kühn and M. Steinhauser, *Corrections of order $O(G_F M_t^2 \alpha_s^2)$ to the ρ parameter*, *Phys. Lett. B* **351** (1995) 331–338, [hep-ph/9502291].
- [10] J. Grigo, J. Hoff, P. Marquard and M. Steinhauser, *Moments of heavy quark correlators with two masses: exact mass dependence to three loops*, *Nucl. Phys. B* **864** (2012) 580–596, [1206.3418].
- [11] J. Blümlein, A. De Freitas, M. Van Hoeij, E. Imamoglu, P. Marquard and C. Schneider, *The ρ parameter at three loops and elliptic integrals*, *PoS LL2018* (2018) 017, [1807.05287].
- [12] S. Abreu, M. Becchetti, C. Duhr and R. Marzucca, *Three-loop contributions to the ρ parameter and iterated integrals of modular forms*, *JHEP* **02** (2020) 050, [1912.02747].
- [13] Y. Schröder and M. Steinhauser, *Four-loop singlet contribution to the rho parameter*, *Phys. Lett. B* **622** (2005) 124–130, [hep-ph/0504055].
- [14] K. G. Chetyrkin, M. Faisst, J. H. Kühn, P. Maierhöfer and C. Sturm, *Four-Loop QCD Corrections to the Rho Parameter*, *Phys. Rev. Lett.* **97** (2006) 102003, [hep-ph/0605201].
- [15] R. Boughezal and M. Czakon, *Single scale tadpoles and $O(G_F m_t^2 \alpha_s^3)$ corrections to the ρ parameter*, *Nucl. Phys. B* **755** (2006) 221–238, [hep-ph/0606232].
- [16] J. J. van der Bij and F. Hoogeveen, *Two Loop Correction to Weak Interaction Parameters Due to a Heavy Fermion Doublet*, *Nucl. Phys. B* **283** (1987) 477–492.
- [17] R. Barbieri, M. Beccaria, P. Ciafaloni, G. Curci and A. Vicere, *Radiative correction effects of a very heavy top*, *Phys. Lett. B* **288** (1992) 95–98, [hep-ph/9205238], [Erratum: *Phys. Lett. B* **312** (1993) 511–511].
- [18] J. Fleischer, O. V. Tarasov and F. Jegerlehner, *Two loop heavy top corrections to the rho parameter: A Simple formula valid for arbitrary Higgs mass*, *Phys. Lett. B* **319** (1993) 249–256.
- [19] J. J. van der Bij, K. G. Chetyrkin, M. Faisst, G. Jikia and T. Seidensticker, *Three loop leading top mass contributions to the rho parameter*, *Phys. Lett. B* **498** (2001) 156–162, [hep-ph/0011373].
- [20] M. Faisst, J. H. Kühn, T. Seidensticker and O. Veretin, *Three loop top quark contributions to the rho parameter*, *Nucl. Phys. B* **665** (2003) 649–662, [hep-ph/0302275].
- [21] J. L. Bourjaily et al., *Functions Beyond Multiple Polylogarithms for Precision Collider Physics*, in *Snowmass 2021*, 3, 2022. 2203.07088.
- [22] P. Nogueira, *Automatic Feynman Graph Generation*, *J. Comput. Phys.* **105** (1993) 279–289.
- [23] B. Ruijl, T. Ueda and J. Vermaseren, *FORM version 4.2*, 1707.06453.
- [24] K. G. Chetyrkin, A. L. Kataev and F. V. Tkachov, *New Approach to Evaluation of Multiloop Feynman Integrals: The Gegenbauer Polynomial x Space Technique*, *Nucl. Phys.* **B174** (1980) 345–377.

- [25] K. G. Chetyrkin and F. V. Tkachov, *Integration by Parts: The Algorithm to Calculate β Functions in 4 Loops*, *Nucl. Phys.* **B192** (1981) 159–204.
- [26] F. V. Tkachov, *A Theorem on Analytical Calculability of Four Loop Renormalization Group Functions*, *Phys. Lett.* **B100** (1981) 65–68.
- [27] A. von Manteuffel and C. Studerus, *Reduze 2 - Distributed Feynman Integral Reduction*, 1201.4330.
- [28] X. Liu, Y.-Q. Ma and C.-Y. Wang, *A Systematic and Efficient Method to Compute Multi-loop Master Integrals*, *Phys. Lett. B* **779** (2018) 353–357, [1711.09572].
- [29] X. Liu and Y.-Q. Ma, *Multiloop corrections for collider processes using auxiliary mass flow*, *Phys. Rev. D* **105** (2022) L051503, [2107.01864].
- [30] Z.-F. Liu and Y.-Q. Ma, *Determining Feynman Integrals with Only Input from Linear Algebra*, *Phys. Rev. Lett.* **129** (2022) 222001, [2201.11637].
- [31] X. Liu and Y.-Q. Ma, *AMFlow: A Mathematica package for Feynman integrals computation via auxiliary mass flow*, *Comput. Phys. Commun.* **283** (2023) 108565, [2201.11669].
- [32] S. Gerhold, *Uncoupling Systems of Linear Ore Operator Equations*, diploma thesis, RISC, J. Kepler University Linz, 2002.
- [33] B. Zürcher, *Rationale Normalformen von pseudo-linearen Abbildungen*, diploma thesis, ETH Zürich, 1994.
- [34] S. A. Abramov and E. V. Zima, *A universal program to uncouple linear systems*, in *Proc. International Conference on Computational Modelling and Computing in Physics*, pp. 16–26, 1996.
- [35] M. van Hoeij, *Factorization of Differential Operators with Rational Functions Coefficients*, *J. Symb. Comput.* **24** (1997) 537–561.
- [36] A. Primo and L. Tancredi, *On the maximal cut of Feynman integrals and the solution of their differential equations*, *Nucl. Phys. B* **916** (2017) 94–116, [1610.08397].
- [37] A. Primo and L. Tancredi, *Maximal cuts and differential equations for Feynman integrals. An application to the three-loop massive banana graph*, *Nucl. Phys. B* **921** (2017) 316–356, [1704.05465].
- [38] P. A. Baikov, *Explicit solutions of the three loop vacuum integral recurrence relations*, *Phys. Lett. B* **385** (1996) 404–410, [hep-ph/9603267].
- [39] H. Frellesvig and C. G. Papadopoulos, *Cuts of Feynman Integrals in Baikov representation*, *JHEP* **04** (2017) 083, [1701.07356].
- [40] E. Remiddi and L. Tancredi, *Differential equations and dispersion relations for Feynman amplitudes. The two-loop massive sunrise and the kite integral*, *Nucl. Phys. B* **907** (2016) 400–444, [1602.01481].

- [41] S. Weinzierl, *Feynman Integrals*. Springer Nature, Cham, Switzerland, 2022, [10.1007/978-3-030-99558-4](https://doi.org/10.1007/978-3-030-99558-4).
- [42] J. Ablinger, J. Blümlein, A. De Freitas, M. van Hoeij, E. Imamoglu, C. G. Raab et al., *Iterated Elliptic and Hypergeometric Integrals for Feynman Diagrams*, *J. Math. Phys.* **59** (2018) 062305, [[1706.01299](https://arxiv.org/abs/1706.01299)].